AIP Advances

Molecular beam epitaxy of TmTe thin films on SrF_2 (111)

Cite as: AIP Advances **12**, 025319 (2022); https://doi.org/10.1063/5.0083276
Submitted: 27 December 2021 • Accepted: 28 January 2022 • Published Online: 11 February 2022

S. Müller, F. Spriestersbach, C.-H. Min, et al.

ARTICLES YOU MAY BE INTERESTED IN

Molecular beam epitaxy of antiferromagnetic $(MnBi_2Te_4)(Bi_2Te_3)$ thin films on BaF_2 (111)
Journal of Applied Physics **128**, 135303 (2020); https://doi.org/10.1063/5.0025933

Properties of topological crystalline insulator $Pb_{0.5}Sn_{0.5}Te$ epitaxial films doped with bismuth
Journal of Applied Physics **131**, 085302 (2022); https://doi.org/10.1063/5.0080329

Structural properties of Bi_2Te_3 topological insulator thin films grown by molecular beam epitaxy on (111) BaF_2 substrates
Journal of Applied Physics **119**, 165303 (2016); https://doi.org/10.1063/1.4947266

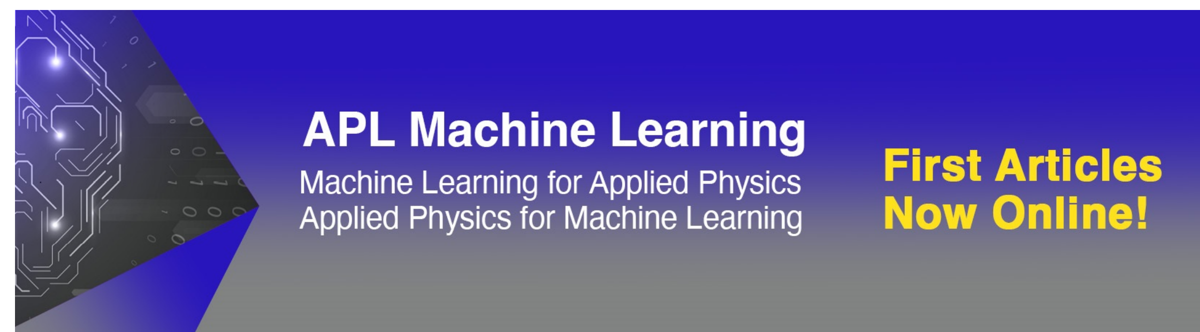

© 2022 Author(s).

Molecular beam epitaxy of TmTe thin films on SrF_2 (111)

Cite as: AIP Advances 12, 025319 (2022); doi: 10.1063/5.0083276
Submitted: 27 December 2021 • Accepted: 28 January 2022 •
Published Online: 11 February 2022

S. Müller[1] F. Spriestersbach,[1] C.-H. Min[2] C. I. Fornari,[1,a)] and F. Reinert[1]

AFFILIATIONS

[1] Experimentelle Physik VII and Würzburg-Dresden Cluster of Excellence ct.qmat, Universität Würzburg, Am Hubland, D-97074 Würzburg, Germany, EU
[2] Institut für Experimentelle und Angewandte Physik, Christian-Albrechts-Universität, Kiel, Germany, EU

[a)] Author to whom correspondence should be addressed: celso.fornari@physik.uni-wuerzburg.de

ABSTRACT

The odd parity nature of $4f$ states characterized by strong spin–orbit coupling and electronic correlations has led to a search for novel topological phases among rare earth compounds, such as Kondo systems, heavy Fermions, and homogeneous mixed-valent materials. Our target system is thulium telluride thin films whose bandgap is expected to be tuned as a function of lattice parameter. We systematically investigate the growth conditions of Tm_xTe_y thin films on SrF_2 (111) substrates by molecular beam epitaxy. The ratio between Te and Tm supply was precisely tuned, resulting in two different crystalline phases, which were confirmed by x-ray diffraction and x-ray photoemission spectroscopy. By investigating the crystalline quality as a function of the substrate temperature, the optimal growth conditions were identified for the desired Tm_1Te_1 phase. Additional low energy electron diffraction and reflective high energy electron diffraction measurements confirm the epitaxial growth of TmTe layers. X-ray reflectivity measurements demonstrate that homogeneous samples with sharp interfaces can be obtained for varied thicknesses. Our results provide a reliable guidance to prepare homogeneous high-quality TmTe thin films and thus serve as a basis for further electronic investigations.

© 2022 Author(s). All article content, except where otherwise noted, is licensed under a Creative Commons Attribution (CC BY) license (http://creativecommons.org/licenses/by/4.0/). https://doi.org/10.1063/5.0083276

I. INTRODUCTION

Topologically nontrivial electronic structures in solids have become a central topic in the field of condensed matter physics since they highlight the importance of the phases of wave-functions in physical properties. Strongly spin–orbit split bands have been scrutinized for insulating systems,[1,2] and the concept has been applied for semimetallic compounds.[3–5] Simultaneously, the research activities for novel topological phases have been initiated among the strongly correlated electron systems (SCES),[6,7] where one can expect further exotic states due to the interplay with strong correlation-driven effects.[8,9] In the case of the prototypical SmB_6, investigations have begun by revisiting the resistance plateau at low temperature ($T < 5$ K)[10,11] described by the Anderson model.[12] Subsequently, the interest has been transferred to semi-metallic Sm-based homogeneous mixed valence (MV) compounds as well.[13,14]

MV systems[15,16] are appropriate materials for topological studies in SCES because inverted bandgaps are expected to be present. The $4f$ states with odd parity lie right at the Fermi-level (E_F), which most likely exhibit hybridization gaps between the localized $4f$ states and conduction band states. Considering the universal hybridization strength between localized $4f$ states and conduction $5d$ states among rare-earth compounds, MV phases are predicted to have higher coherence temperature,[17,18] which makes the realization in the experiment more feasible.

Although diverse $4f$ compounds have claimed to be topologically non-trivial, there is a scarcity of angle-resolved photoemission spectroscopy (ARPES) investigations, which could directly prove the Dirac cone.[19] However, recent slab calculation analyses have demonstrated solutions to observe the Dirac points in fcc-structured MV compounds by looking at different surface orientations.[20,21] Hence, a MV system in a fcc structure is a very promising material for such studies.

Our ultimate goal is to control the evolution of the hybridized gap inversion, which entails a metal–insulator transition (MIT). Thulium monochalcogenides ($TmSe_{1-x}Te_x$) are our choice of material for this study.[22–24] This is a unique MV system having an antiferromagnetic ground state ($T_N < 4$ K).[25] By applying either

© Author(s) 2022

pressure or chemical substitution, the MIT occurs in $TmSe_{1-x}Te_x$ keeping the fcc structure and smooth connections in thermopower and specific heat.[26,27] The MIT also entails the variation in both the valence of Tm, v_{Tm}, from 2.65 ± 0.05 (TmSe) to 2.01 ± 0.01 (TmTe)[28–31] and the crystalline lattice constant from a_{TmSe} = 5.71 Å to a_{TmTe} = 6.35 Å.[28,32,33] Thus, applying pressure or chalcogen substitution plays almost an identical role.

Instead of applying pressure or chemical substitution, we implement the thin film growth of TmTe on a substrate with a smaller lattice constant than the bulk TmTe, with the aim of applying compressive strain.[34] By tuning the thickness of the samples, MIT and a change in v_{Tm} are expected. Another advantage of the film growth approach is that various oriented surfaces become accessible by choosing a suitable substrate.[35] The natural cleaving plane of Tm monochalcogenide bulk crystals limits the access to the (001) orientation.

The growth of TmTe thin films has not yet been extensively investigated.[28,35] Thus, in this study, we systematically study the growth behavior of TmTe thin films on the (111) surface of strontium fluoride (SrF_2) substrates, which has a lattice constant of a_{SrF_2} = 5.7996 Å. SrF_2 has a cubic structure with weak bonds between the fluorine atoms along the [111] direction, such as CaF_2 and BaF_2.[36] Our grown films have been investigated as functions of Tm and Te fluxes and substrate temperature. Structural and electronic characterization studies were performed using x-ray diffraction (XRD), x-ray reflectivity (XRR), x-ray photoemission spectroscopy (XPS), reflection high-energy electron diffraction (RHEED), and low-energy electron diffraction (LEED). Depending on the growth parameters, different Tm_xTe_y stoichiometries and modes of growth have been obtained. We identify a narrow window of growth parameters to obtain epitaxial Tm_1Te_1 films with a layer-by-layer growth mode.

II. CRYSTALLINE PHASES OF THULIUM TELLURIDE

Thulium telluride has been reported to exist in different stoichiometric phases, with Tm_1Te_1 and Tm_2Te_3 being the more common ones. These phases are characterized by different stoichiometries, resulting in a change in the crystalline structure, the lattice constant, and the valence of thulium.[37]

Kaldis *et al.*[37] presented a phase diagram derived from their studies on bulk crystal preparation. The first phase is the Tm-monotelluride (Tm_1Te_1) with its simple rock-salt (space group, Fm-3m) structure (Fig. 1). In this stoichiometry, TmTe is suggested to be a pure divalent Tm^{2+}. The reported lattice constant is a_0 = 6.36 Å[37] for bulk crystals and a_0 = 6.34 Å[28] for the powder sample.

The second phase occurs for a strong Tm-deficiency (or excess of Te), leading to the crystallization of Tm_2Te_3 ($Tm_{0.68}Te$) with an orthorhombic Sc_2S_3 structure (space group, Fddd). This structure is a super-structure of the rock-salt type, where the stoichiometry is accommodated by the presence of ordered Tm vacancies,[38] as depicted in the cut along the [620] direction in Fig. 1(b). The lattice constants are reported to be a' = 25.631(30) Å, b' = 12.060(20) Å, and c' = 8.541(5) Å with the corresponding NaCl lattice constant of the subcell a_0 = 6.0400(8) Å.[37–39] The orientation of the rock-salt sub-cell is such that its [101] ([010]) direction is parallel to the [100] ([010]) direction of the Sc_2S_3 structure. This results in the accordance of the NaCl (111) planes with the Sc_2S_3 (022) and (620) planes (see Fig. 1). In this phase, the valence of Tm is very close to tri-valence.

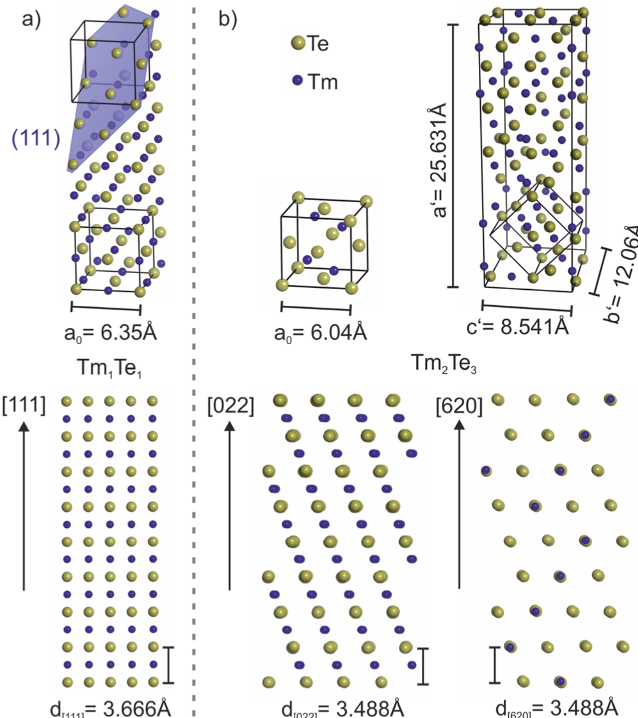

FIG. 1. Representation of the crystalline structures of the phases Tm_1Te_1 in (a) and Tm_2Te_3 in (b) and their equivalent orientations. The blue layer in (a) indicates the (111) plane in the NaCl structure.

III. EXPERIMENTAL DETAILS

For this work, Tm_xTe_y thin films were grown on freshly cleaved SrF_2 (111) substrates using effusion cells charged with Tm (99.999%) and Te (99.9999%). The cells were operated around 850 and 280 °C for Tm and Te, respectively. The beam equivalent pressure (BEP) is monitored by placing an ion gauge at the substrate position before and after each growth. The average BEP value is used as reference. We define the parameter $\Phi_R = BEP_{Te}/BEP_{Tm}$ to determine the ratio between the molecular fluxes of tellurium and thulium. Hence, $\Phi_R = 0$ corresponds to a pure thulium film. In this work, BEP_{Tm} was kept constant, while the influence of Φ_R and substrate temperature was investigated. The base pressure of the growth chamber is 5×10^{-11} mbar, and it does not exceed 3×10^{-8} mbar during deposition. The SrF_2 substrates are pre-heated at 400 °C for 30 min before starting deposition. The film surface is monitored *in situ* and during the growth using a reflection high-energy electron diffraction (RHEED) system. The RHEED system is equipped with a 30 keV electron gun and a CCD camera installed in front of the fluorescent screen. The crystalline structure representations (Fig. 1) were drawn using the software package VESTA.[40]

The x-ray diffraction (XRD) and x-ray reflectometry (XRR) curves were acquired using a Bruker high resolution x-ray

© Author(s) 2022

diffractometer providing Cu K_α radiation with λ = 1.540 56 Å, equipped with a Göbel mirror, a Ge (220) monochromator, and a scintillator detector. In order to extract quantitative information, the XRR curves were calculated using the GenX software package.[41]

X-ray photoelectron spectroscopy (XPS) experiments were performed *in situ* directly after growth. The photoemission chamber is connected by ultra-high vacuum lines to the molecular beam epitaxy (MBE) chamber and is equipped with a Mg anode (Mg K_α 1253.7 eV) and a Scienta SES200 photoelectron analyzer. Low energy electron diffraction (LEED) measurements were carried out *in situ* using a Thermo VG Scientific standard LEED system.

IV. RESULTS AND DISCUSSION

The growth of the Tm_xTe_y films was investigated in different directions. First, a series of films was prepared with different Te to Tm beam flux ratios (Φ_R) in order to obtain the desired stoichiometry. Subsequently, by fixing Φ_R to obtain a single phase Tm_1Te_1, a series was prepared by varying the substrate temperature. The growth parameters to obtain epitaxial layers with high-crystalline quality were determined. By carefully selecting the best experimental conditions to obtain these layers, we investigate the growth dynamics of the samples.

However, since the structural analysis was performed *ex situ* by XRD and XRR and Tm compounds are very sensitive to the adsorption of molecules and gases, it was necessary to first find a proper protective capping layer to prevent oxidation and thus the destruction of the crystalline structure of the films. For this, three different compounds were tested as a protective cap on the Tm_xTe_y films: Te, Bi_2Te_3, and BaF_2. Due to the small lattice-mismatch, BaF_2 and Bi_2Te_3 serve very well as protective capping layers, growing homogeneously on top of TmTe with substrate temperature fixed at 250 °C. We also found out that Bi_2Te_3 grows epitaxially with the Bi_2Te_3 (0001) surface parallel to the (111) surface of TmTe. Pure tellurium, on the other hand, requires a more delicate approach. Depending on the substrate temperature, Te deposition results in different structures. At 240 °C, pure Te does not stick on the surface,[42,43] while at room temperature, it grows as columns that are permeable to oxygen. In order to have a homogeneous coverage, the substrate temperature has to be kept around 80 °C. The benefit of Te is the easy removal of the capping layer by thermal desorption. In this work, we decided to use BaF_2 as a protective capping layer because of the long-term reliability in terms of protecting the crystal structure of the films, the easy growth, and the sufficiency of very thin caps. In addition, BaF_2 is highly insulating and transparent from the ultraviolet to the far infra-red, which could facilitate transport and optical investigations.

A. Tellurium supply

To explore the possibility of different phases of Tm_xTe_y, our first approach was to vary the amount of Te supply while keeping the beam flux of thulium constant at BEP_{Tm} = 2.4 $\times 10^{-7}$ mbar. For this series, the substrate temperature T_{sub} = 425 °C and the deposition time t_{growth} = 60 min were kept constant.

The surface of the films was investigated by RHEED after 10 min of deposition. Figure 2 displays the RHEED patterns acquired for samples prepared with different Φ_R values. For Φ_R = 1.78, single dots with high intensity are observable, indicating the nucleation of three-dimensional islands on the surface. The observed RHEED patterns resemble the strained Stranski–Krastanov patterns of GaAs quantum dots.[44] For a flux ratio of Φ_R = 2.68, the sharp dots appear elongated along the surface normal, indicating that the surface is becoming flatter and smoother. Increasing the extra Te supply even more leads to a different ordering of the surface. For Φ_R = 3.16, several dots appear vertically aligned, while for Φ_R = 4.12, polycrystalline domains start to be formed, as indicated by dashed circles in this figure. A diagonal order of diffraction spots is visible for $\Phi_R \leq 2.68$, while for $\Phi_R \geq 3.16$, a vertical order is present. Blue dots in Fig. 2 indicate this ordering.

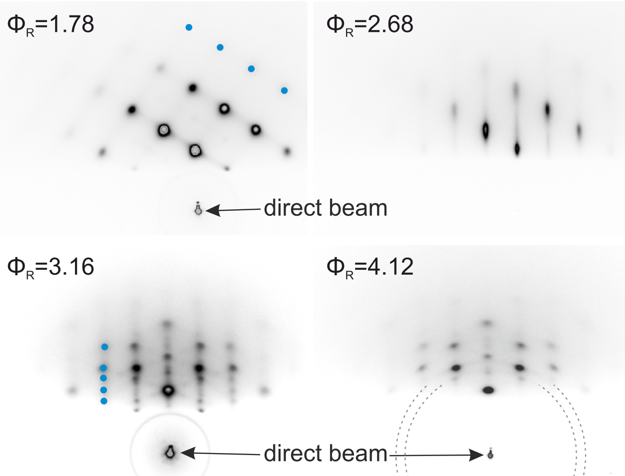

FIG. 2. Search for the optimal Φ_R value for the epitaxial growth. RHEED patterns acquired along the [$\bar{2}$11] azimuth after 10 min of deposition of thulium telluride layers on SrF_2 (111) substrates as a function of Φ_R beam flux ratio are shown. The substrate temperature was kept constant at 425 °C.

The crystal structures were determined by XRD measurements and are shown in Fig. 3(a). All the measurements are normalized to the height of the respective substrate peak SrF_2 (222) and aligned to its theoretical position at 2θ = 54.7869° for Cu K_α. The small peak around 2θ = 49.15° represents the same substrate peak but induced by the remnant Cu K_β line of the x-ray gun. Depending on Φ_R, the diffraction curves present an additional peak either around 2θ = 49.6° (for $\Phi_R \leq 2.68$) or around 2θ = 52.3° (for $\Phi_R \geq 3.01$). These peaks correspond to Tm_1Te_1 (222) and the overlap of Tm_2Te_3 (044) and (1240), respectively. These Tm_2Te_3 orientations, which correspond to the rock-salt sub-lattice [111] orientation, are also confirmed by the presence of its (022) and (620) Bragg peaks around 2θ = 25.5° (not shown here). The observation of the overlap of (1200) and (004) reflections around 2θ = 42.2°, respectively, corresponding to NaCl sub-lattice orientations [101] and [$\bar{1}$01] points out a second growth orientation of Tm_2Te_3, while for Tm_1Te_1, only the [111] orientation is observed.

The clear presence of distinct Bragg peaks as a function of Φ_R allows us to determine a sharp threshold to obtain a single phase Tm_1Te_1 or Tm_2Te_3. To compare these results to reported lattice constants from the literature,[37] we calculated the lattice constant

© Author(s) 2022

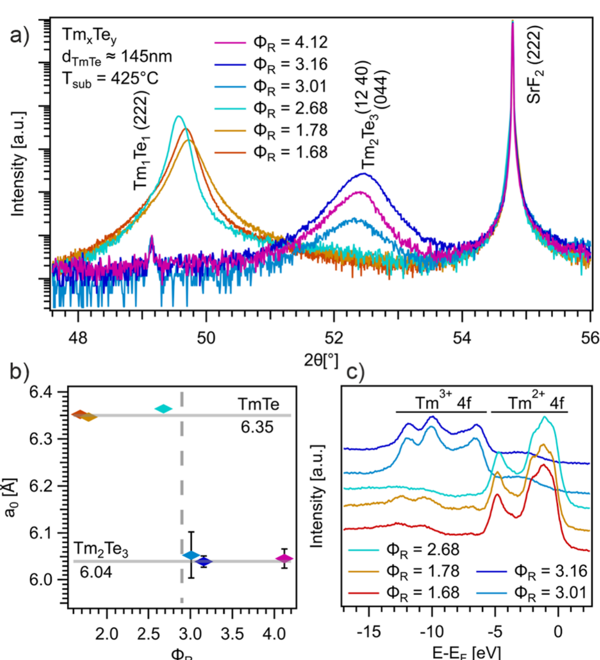

FIG. 3. Structural and electronic characterization of thulium telluride layers prepared with different Φ_R values. (a) X-ray diffraction curves recorded in the vicinity of the SrF_2 (222) diffraction peak. (b) Experimental lattice constants obtained from (a). The solid lines indicate the bulk lattice constant of the respective phases. (c) X-ray photoelectron spectroscopy results acquired right after the growth of the films.

from the peak position assuming a cubic lattice for both phases, as shown in Fig. 1. The dependence between the cubic lattice constant and Φ_R is plotted in Fig. 3(b). The error bars represent the propagation of uncertainty of the fitting parameter errors from Voigt curves. The straight lines serve as comparison to the literature bulk values for both Tm_xTe_y phases, while the vertical dashed line marks the threshold in Φ_R between both phases.

Thulium valence was investigated by XPS as a function of Φ_R. Figure 3(c) shows the photoemission spectra of the Tm 4*f* levels acquired *in situ* right after the growth of the samples. The spectra show a clear valence transition from Tm^{2+} to Tm^{3+} when increasing Φ_R above 2.68 and thus corroborate the threshold found on the structural analysis. The different valencies match exactly the phases of thulium telluride observed in Fig. 3(a). Even though the Te sticking coefficient tends to decrease dramatically for substrate temperatures above 200 °C[42,43] and for other rock-salt semiconductors, such as PbTe and SnTe, a single stoichiometry 1:1 is always reached, and thulium telluride layers can present very distinct phases depending on the growth conditions. Based on these results, for a reliable growth of the Tm_1Te_1 phase, Φ_R was defined to a value of 2.0 far enough from the threshold to the other phase.

B. Substrate temperature

The ideal extra Te supply (Φ_R) to obtain a pure Tm_1Te_1 phase was defined to be 2.0. Thus, for further investigations, we kept $\Phi_R \approx 2.0$ and varied the substrate temperature T_{sub} between 350 and 575 °C. The deposition time was fixed as 60 min for all samples.

Figure 4 displays the RHEED patterns recorded after 5 min of deposition of thulium telluride on SrF_2 (111) substrates for different T_{sub} values. At low substrate temperature (T_{sub} = 350 °C), the growing layer presents a poly-crystalline texture with faint spots. This indicates that TmTe clusters crystallize on the surface of the substrate randomly oriented. By increasing the substrate temperature to T_{sub} = 425 °C and thus providing more thermal energy to the system, the acquired RHEED pattern indicates the formation of oriented islands on the substrate. For films grown at T_{sub} = 550 °C, a mixture of streaky RHEED patterns modulated with dots indicates that the growing surface is becoming flatter and smoother. A pure layer-by-layer growth mode was reached at T_{sub} = 575 °C, where no signs of island growth were observed. These RHEED patterns, observed at different T_{sub} values, clearly show that substrate temperature plays an essential role in determining the crystalline quality and growth dynamics of these layers.

To determine the crystalline structure of these samples, XRD measurements were performed. The results are presented in Fig. 5(a). For the whole investigated range of substrate temperature, the measured curves present a single Tm_1Te_1 phase. The inset in (a) shows rocking curves recorded around the Tm_1Te_1 (222) Bragg peak. It can be observed that by increasing the substrate temperature, a narrowing of the full width at half maximum (FWHM) is reached, indicating an enhancement of the crystalline quality. The measured lattice constant stays around a_0 = 6.35 Å. Figure 5(b) shows the calculated rock-salt lattice constants a_0 and the extracted full width of half maximum (FWHM) from rocking curves. The dotted lines in (b) serve as guides to the eye. Since the FWHM can be seen as a crystal quality factor, its exponential decay with increasing substrate temperature is a clear indication of improved crystalline quality at higher T_{sub}. The lattice constants, extracted from the XRD measurements, present a slight increase by raising the substrate temperature.

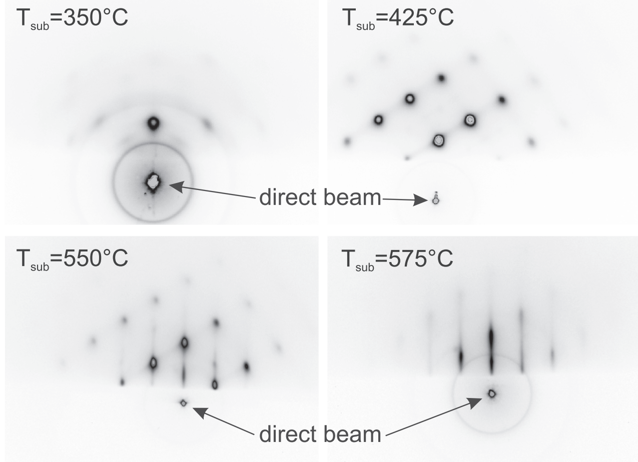

FIG. 4. Investigation of the influence of T_{sub} on the growth of TmTe films. RHEED patterns acquired along the [$\bar{2}$11] azimuth after 5 min of deposition of thulium telluride on SrF_2 (111) substrates as a function of the substrate temperature are shown. For all samples, Φ_R was kept around 2.0.

© Author(s) 2022

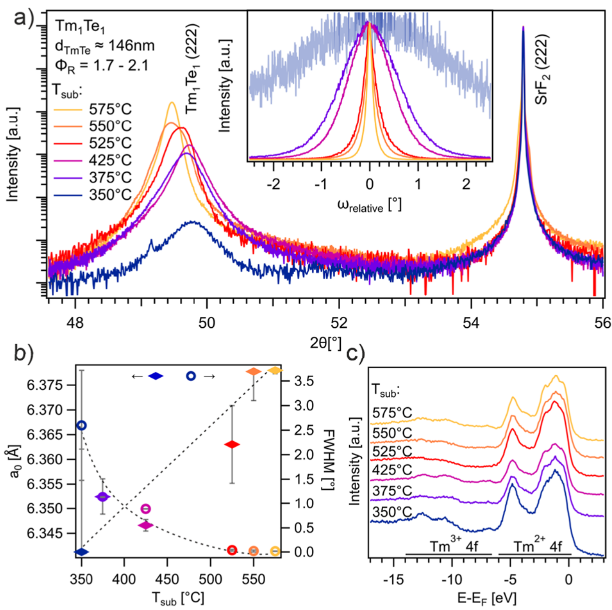

FIG. 5. Structural and electronic characterization of thulium telluride layers prepared at different substrate temperatures and Φ_R fixed at 2.0. (a) X-ray diffraction curves recorded in the vicinity of the SrF_2 (222) diffraction peak. (b) Experimental full width at half maximum values and lattice constants obtained from the TmTe (222) diffraction peak shown in (a). The dotted lines serve as guides to the eye. (c) X-ray photoelectron spectroscopy results acquired *in situ* right after the growth of the samples.

The lattice constant a_0 is calculated using the Bragg equation with the peak position of Tm_1Te_1 (222). Since this peak position is determined by the spacing between the (222) inter-layers, stacked along the out-of-plane direction [111], an increase in the lattice constant a_0 represents a tensile deformation out-of-plane. This could occur due to the reinforced acceptance at higher temperatures of the substrate induced compressive in-plane strain, which would lead to the tensile strain out-of-plane to keep the unit cell volume constant. In order to investigate the electronic structure of these samples, XPS measurements were performed and are presented in Fig. 5(c). All measured samples exhibit spectra with nearly Tm^{2+} valence of the $4f$ states, except for the sample with poly-crystalline texture that was prepared at the lowest T_{sub} value. In this case, a small intensity of the density of states corresponding to Tm^{3+} can be observed. Despite the sample being prepared at T_{sub} = 350 °C, XPS also confirms the right Tm_1Te_1 phase.

C. Epitaxial growth with optimal conditions

In order to obtain more information about the growth dynamics of TmTe, films with varied thicknesses were prepared. For this, the experimental conditions to obtain a single phase with high crystalline order were used. The substrate temperature was set to T_{sub} = 575 °C and the Tm/Te flux ratio to Φ_R = 2.0. Two samples were prepared with a deposition time of 20 and 60 min, respectively.

Figure 6(a) shows LEED images acquired *in situ* at 53 and 75 eV from a fresh surface of a 1250 Å thick TmTe film. Since the atomic order on the (111) plane of the rock-salt structure is hexagonal, as shown in Fig. 1, the LEED measurements confirm the epitaxial growth. No signs of surface reconstruction can be observed, and the sharp spots with low background intensity indicate a highly oriented surface. RHEED measurements acquired from the same sample are presented in Fig. 6(b). The presence of only two equivalent azimuths, rotated by 30° from each other, confirms a single domain of our layers. The streaky RHEED patterns with low background intensity indicate that a smooth and flat surface is exposed. The RHEED intensity [blue box in Fig. 6(b)] was monitored from the beginning of deposition, and Fig. 6(c) shows the graph of intensity vs time. From the instant when

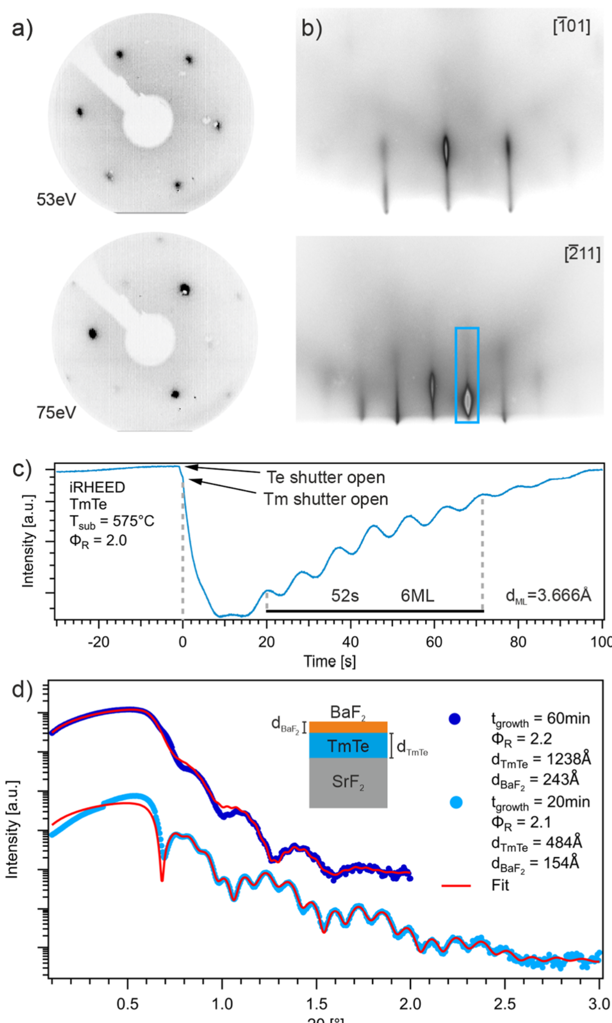

FIG. 6. High-quality epitaxial layers of Tm_1Te_1 grown on SrF_2 (111) substrates. (a) LEED images of a 1250 Å thick TmTe film acquired with 53 and 75 eV. (b) RHEED patterns acquired after 60 min of deposition of TmTe along two different azimuths. (c) RHEED intensity recorded as a function of time, showing a layer-by-layer deposition since the initial stages of epitaxy. (d) XRR curves of TmTe films grown on SrF_2 substrates together with the calculated curves. The samples were covered with a BaF_2 protective capping layer.

© Author(s) 2022

the Te and Tm shutters are open, oscillations in the RHEED patterns can be observed. A maximum of the oscillation occurs when a complete and closed layer is grown. Clear oscillations can be observed once the growth starts. Considering the thickness of one monolayer along the [111] direction as $d_{ML,[111]} = a_0/\sqrt{3} = 3.666$ Å, a growth rate of 0.42 Å/s (0.12 ML/s) is obtained.

The *ex situ* XRR measurements obtained from samples grown for 20 and 60 min are presented in Fig. 6(d). The samples were covered by a protective BaF_2 capping layer to avoid surface contamination. The software package GenX was used to calculate the XRR curves in order to extract quantitative information. The presence of pronounced and clear interference fringes indicates a homogeneous layer with smooth interfaces over the whole substrate area. The film grown for 60 min results in a thickness of $d_{TmTe} = 1238$ Å and thus a growth rate of 0.34 Å/s, while the thickness of the film grown for 20 min results in roughly a third of the previous value, namely, $d_{TmTe} = 484$ Å (0.40 Å/s). The thickness of the capping layer is also extracted as $d_{BaF_2} = 243$ Å and $d_{BaF_2} = 154$ Å, respectively. These results indicate that at specific growth conditions, a layer-by-layer growth mode can be obtained. By controlling the deposition time, homogeneous layers with smooth interfaces can be prepared with different thicknesses.

V. SUMMARY

In this work, the molecular beam epitaxy of Tm_xTe_y was systematically investigated on SrF_2 (111) substrates by co-evaporation of Tm and Te. Structural analysis demonstrates that two different stoichiometric phases of thulium telluride can be obtained depending on the extra Te supply: TmTe ($2.68 < \Phi_R$) and Tm_2Te_3 ($\Phi_R > 3.01$). The existence of these distinct phases is also supported by XPS measurements. For thulium monotelluride, the crystalline quality significantly improves by increasing the substrate temperature to $T_{sub} = 575\,^{\circ}$C. At these conditions, RHEED measurements revealed a layer-by-layer growth mode that remains throughout the whole deposition. XRR measurements demonstrate homogeneous layers, with sharp and smooth interfaces. Our results provide a reliable guidance to prepare homogeneous high-quality TmTe thin films and thus serve as a basis for further electronic investigations. This is of great interest for the examination of new non-trivial topological phases in strongly correlated systems based on thulium chalcogenides.

ACKNOWLEDGMENTS

We acknowledge financial support from the DFG through Grant No. SFB1170 "ToCoTronics" (Project C06) and the Würzburg-Dresden Cluster of Excellence on Complexity and Topology in Quantum Matter *ct.qmat* (EXC 2147, Project-ID 390858490). C.I.F. acknowledges the Hallwachs-Röntgen Postdoc Program of ct.qmat. This publication was supported by the Open Access Publication Fund of the University of Wuerzburg.

AUTHOR DECLARATIONS

Conflict of Interest

The authors declare no conflict of interest.

DATA AVAILABILITY

The data that support the findings of this study are available from the corresponding author upon reasonable request.

REFERENCES

[1] L. Fu and C. L. Kane, Phys. Rev. B **76**, 045302 (2007).
[2] M. König, S. Wiedmann, C. Brüne, A. Roth, H. Buhmann, L. W. Molenkamp, X.-L. Qi, and S. Zhang, Science **318**, 766 (2007).
[3] B.-J. Yang and N. Nagaosa, Nat. Commun. **5**, 4898 (2014).
[4] C.-H. Min, H. Bentmann, J. N. Neu, P. Eck, S. Moser, T. Figgemeier, M. Ünzelmann, K. Kissner, P. Lutz, R. J. Koch *et al.*, Phys. Rev. Lett. **122**, 116402 (2019).
[5] M. Ünzelmann, H. Bentmann, T. Figgemeier, P. Eck, J. N. Neu, B. Geldiyev, F. Diekmann, S. Rohlf, J. Buck, M. Hoesch *et al.*, Nat. Commun. **12**, 3650 (2021).
[6] M. Dzero, K. Sun, V. Galitski, and P. Coleman, Phys. Rev. Lett. **104**, 106408 (2010).
[7] B. Roy, J. D. Sau, M. Dzero, and V. Galitski, Phys. Rev. B **90**, 155314 (2014).
[8] D. Chowdhury, I. Sodemann, and T. Senthil, Nat. Commun. **9**, 1766 (2018).
[9] M. M. Otrokov, I. I. Klimovskikh, H. Bentmann, D. Estyunin, A. Zeugner, Z. S. Aliev, S. Gaß, A. U. B. Wolter, A. V. Koroleva, A. M. Shikin *et al.*, Nature **576**, 416 (2019).
[10] S. Wolgast, Ç. Kurdak, K. Sun, J. W. Allen, D.-J. Kim, and Z. Fisk, Phys. Rev. B **88**, 180405(R) (2013).
[11] C.-H. Min, P. Lutz, S. Fiedler, B. Y. Kang, B. K. Cho, H.-D. Kim, H. Bentmann, and F. Reinert, Phys. Rev. Lett. **112**, 226402 (2014).
[12] P. W. Anderson, Phys. Rev. **124**, 41 (1961).
[13] C.-J. Kang, H. C. Choi, K. Kim, and B. I. Min, Phys. Rev. Lett. **114**, 166404 (2015).
[14] D. Kasinathan, K. Koepernik, L. H. Tjeng, and M. W. Haverkort, Phys. Rev. B **91**, 195127 (2015).
[15] F. D. M. Haldane, Phys. Rev. B **15**, 2477 (1977).
[16] C. M. Varma, Phys. Rev. B **102**, 155145 (2020).
[17] J. Werner and F. F. Assaad, Phys. Rev. B **89**, 245119 (2014).
[18] C.-H. Min, F. Goth, P. Lutz, H. Bentmann, B. Y. Kang, B. K. Cho, J. Werner, K.-S. Chen, F. Assaad, and F. Reinert, Sci. Rep. **7**, 11980 (2017).
[19] M. Xia, J. Jiang, Z. R. Ye, Y. H. Wang, Y. Zhang, S. D. Chen, X. H. Niu, D. F. Xu, F. Chen, X. H. Chen *et al.*, Sci. Rep. **4**, 5999 (2014).
[20] C.-J. Kang, D.-C. Ryu, J. Kim, K. Kim, J.-S. Kang, J. D. Denlinger, G. Kotliar, and B. I. Min, Phys. Rev. Mater. **3**, 081201 (2019).
[21] D.-C. Ryu, J. Kim, K. Kim, C.-J. Kang, J. D. Denlinger, and B. I. Min, Phys. Rev. Res. **2**, 012069 (2020).
[22] E. Kaldis, B. Fritzler, and W. Peteler, Z. Naturforsch., A **34**, 55 (1979).
[23] U. Köbler, K. Fischer, K. Bickmann, and H. Lustfeld, J. Magn. Magn. Mater. **24**, 34 (1981).
[24] H. Boppart, J. Magn. Magn. Mater. **47–48**, 436 (1985).
[25] H. B. Møller, S. M. Shapiro, and R. J. Birgeneau, Phys. Rev. Lett. **39**, 1021 (1977).
[26] J. Derr, G. Knebel, G. Lapertot, B. Salce, M.-A. Méasson, and J. Flouquet, J. Phys.: Condens. Matter **18**, 2089 (2006).
[27] O. B. Tsiok, L. G. Khvostantsev, A. V. Golubkov, I. A. Smirnov, and V. V. Brazhkin, Phys. Rev. B **90**, 165141 (2014).
[28] R. Suryanarayanan, G. Güntherodt, J. L. Freeouf, and F. Holtzberg, Phys. Rev. B **12**, 4215 (1975).
[29] A. Bianconi, S. Modesti, M. Campagna, K. Fischer, and S. Stizza, J. Phys. C: Solid State Phys. **14**, 4737 (1981).
[30] T. Kinoshita, Y. Ufuktepe, K. G. Nath, S. Kimura, H. Kumigashira, T. Takahashi, T. Matsumura, T. Suzuki, H. Ogasawara, and A. Kotani, J. Electron Spectrosc. Relat. Phenom. **88–91**, 377 (1998).
[31] I. Jarrige, H. Ishii, Y. Q. Cai, J.-P. Rueff, C. Bonnelle, T. Matsumura, and S. R. Shieh, Phys. Rev. B **72**, 075122 (2005).
[32] M. Campagna, E. Bucher, G. K. Wertheim, D. N. E. Buchanan, and L. D. Longinotti, Phys. Rev. Lett. **32**, 885 (1974).

© Author(s) 2022

[33]B. Batlogg, H. R. Ott, E. Kaldis, W. Thöni, and P. Wachter, Phys. Rev. B **19**, 247 (1979).
[34]C.-W. Liu, J.-J. Dai, S.-K. Wu, N.-Q. Diep, S.-H. Huynh, T.-T. Mai, H.-C. Wen, C.-T. Yuan, W.-C. Chou, J.-L. Shen *et al.*, Sci. Rep. **10**, 12972 (2020).
[35]X. Cai, Z. Lu, Z. Xu, F. Meng, Q. Zhang, L. Gu, J. Feng, S.-H. Ji, N. Li, and X. Chen, J. Phys. Chem. C **125**, 15465 (2021).
[36]L. He, X. Kou, and K. L. Wang, Phys. Status Solidi RRL **7**, 50 (2013).
[37]E. Kaldis, E. Jilek, and H. Spychiger, J. Less-Common Met. **93**, 399 (1983).
[38]J. P. Dismukes and J. G. White, Inorg. Chem. **4**, 970 (1965).
[39]I. Hinz, P. Kuhn, U. Vetter, and E. Warkentin, Sc, Y, *La-Lu Rare Earth Elements, Part of the Gmelin Handbook of Inorganic Chemistry* (Springer, 1986), ISBN: 978-3-662-06366-8.
[40]K. Momma and F. Izumi, J. Appl. Crystallogr. **44**, 1272 (2011).
[41]M. Björck and G. Andersson, J. Appl. Crystallogr. **40**, 1174 (2007).
[42]C. I. Fornari, P. H. O. Rappl, S. L. Morelhão, and E. Abramof, J. Appl. Phys. **119**, 165303 (2016).
[43]D. S. H. Liu, M. Hilse, and R. Engel-Herbert, J. Vac. Sci. Technol. A **39**, 023413 (2021).
[44]G. Balakrishnan, J. Tatebayashi, A. Khoshakhlagh, S. H. Huang, A. Jallipalli, L. R. Dawson, and D. L. Huffaker, Appl. Phys. Lett. **89**, 161104 (2006).

© Author(s) 2022